4056–4067 *Nucleic Acids Research, 2014, Vol. 42, No. 6* *Published online 20 January 2014*
doi:10.1093/nar/gkt1418

Engineering of a conditional allele reveals multiple roles of XRN2 in *Caenorhabditis elegans* development and substrate specificity in microRNA turnover

Takashi S. Miki[1,†], Stefan Rüegger[1,2,†], Dimos Gaidatzis[1,3], Michael B. Stadler[1,3] and Helge Großhans[1,*]

[1]Friedrich Miescher Institute for Biomedical Research, Maulbeerstrasse 66, CH-4058 Basel, Switzerland, [2]University of Basel, Petersplatz 1, CH-4003 Basel, Switzerland and [3]Swiss Institute of Bioinformatics, Maulbeerstrasse 66, CH-4058 Basel, Switzerland

Received October 28, 2013; Revised December 20, 2013; Accepted December 24, 2013

ABSTRACT

Although XRN2 proteins are highly conserved eukaryotic 5′→3′ exonucleases, little is known about their function in animals. Here, we characterize *Caenorhabditis elegans* XRN2, which we find to be a broadly and constitutively expressed nuclear protein. An *xrn-2* null mutation or loss of XRN2 catalytic activity causes a molting defect and early larval arrest. However, by generating a conditionally mutant *xrn-2ts* strain *de novo* through an approach that may be also applicable to other genes of interest, we reveal further functions in fertility, during embryogenesis and during additional larval stages. Consistent with the known role of XRN2 in controlling microRNA (miRNA) levels, we can demonstrate that loss of XRN2 activity stabilizes some rapidly decaying miRNAs. Surprisingly, however, other miRNAs continue to decay rapidly in *xrn-2ts* animals. Thus, XRN2 has unanticipated miRNA specificity *in vivo*, and its diverse developmental functions may relate to distinct substrates. Finally, our global analysis of miRNA stability during larval stage 1 reveals that miRNA passenger strands (miR*s) are substantially less stable than guide strands (miRs), supporting the notion that the former are mostly byproducts of biogenesis rather than a less abundant functional species.

INTRODUCTION

XRN2 proteins constitute a family of eukaryotic 5′→3′ exoribonucleases that have various RNA substrates (1). For instance, in yeast, where XRN2 has been particularly well studied and is commonly known as Rat1p, it is involved in processing of ribosomal RNAs and small nucleolar RNAs (2–6), transcriptional termination (7) and degradation of aberrant transfer RNAs (8), among other functions. The diversity of substrates *in vivo* is reflected by relaxed substrate specificity *in vitro* where Rat1p processively degrades 5′ monophosphorylated RNAs that lack strong secondary structures to mononucleotides (9,10). The catalytic site of XRN2/Rat1p contains seven acidic amino acids, which form a pocket for a divalent cation (Mg^{2+} or Mn^{2+}) required for the exoribonuclease activity (11).

A paralogous enzyme, Xrn1p, exists in the yeast cytoplasm (12), where it is involved in degradation of decapped mRNAs (13). Single orthologues of XRN1 and XRN2, respectively, are also found in animals, and it is assumed that distinct localization and the resulting division of labor that characterize yeast Xrn1p and Rat1p (14) also apply to their orthologues in other organisms, although this has not yet been investigated systematically. A nuclear localization signal present in Rat1p is not conserved in XRN2 orthologues of other species (14), but nuclear RNAs such as pre-mRNAs and 5.8S and 18S ribosomal RNAs have been reported as common substrates of XRN2 in yeast and other species [reviewed in (15)]

* To whom correspondence should be addressed. Tel: +41 61 697 6580; Fax: +41 61 697 3976; Email: helge.grosshans@fmi.ch

†These authors contributed equally to the paper as first authors.

In *Caenorhabditis elegans*, the single XRN2-type protein was found to function in degradation of mature microRNAs (miRNAs) (16). These short (~22 nt) non-coding RNAs are derived from longer precursor transcripts, from which two successive processing steps release a ~22 nt duplex RNA consisting of an miRNA guide (miR) bound to an miRNA passenger (miR*) strand (17). This duplex is loaded onto an Argonaute protein and the guide strand retained, whereas the passenger strand is released and presumably discarded. The designation of miR and miR* was initially based on their relative abundance, with the more abundant strand assumed functional and thus designated miR. However, individual miR*s have also been shown to be functional [reviewed in (18)], so that in recent times the use of two suffixes indicating the 'arm' of the precursor transcript from which an miRNA is derived, i.e. −3p or −5p, has become more common. At any rate, miRNA-Argonaute complexes can bind to partially complementary sequences in 3′-untranslated regions (3′-UTRs) of mRNAs to repress their translation and induce their degradation (19). They thus regulate a large number of genes, affording them, as a class, important roles in animal development and pathology (20).

Two lines of evidence support a function of XRN2 in the degradation of mature miRNAs (16). First, *C. elegans* lysates containing wild-type levels of XRN2 were more active in decay of naked synthetic and Argonaute-associated miRNAs than XRN2-depleted lysates. Second, depletion of XRN2 by RNA interference (RNAi) yielded increased steady-state levels of a number of endogenous miRNAs. In these latter experiments, however, the levels of some miRNAs were unchanged. Because RNAi may be inefficient in certain tissues or at certain times, it remained unknown whether this reflected true substrate specificity or a technical limitation of the experiment.

Despite prominent molecular functions, the roles of XRN2 in animal development largely remain to be explored (15). In mice and humans, over-expression of XRN2 has been implicated as a risk factor for a specific type of lung cancer (21), but a molecular basis remains to be established. In *C. elegans*, XRN2, encoded by the *xrn-2* gene, was found in a genome-wide RNAi screen for factors involved in molting (22), the process in which worms synthesize a new and shed their old cuticle. Molting occurs once at the end of each of the four larval stages, L1 through L4, (23) and Frand *et al*. (22) found that *xrn-2* depleted animals were unable to shed the cuticle from the pharynx at the final (L4) molt. Consistent with this phenotype, a putative *xrn-2* promoter, with only limited spatial activity as assayed by a Green Fluorescent Protein (GFP) reporter, was active in myoepithelial cells that secrete the pharyngeal cuticle (22). Promoter activity also occurred in other cells implicated in molting, including a particular pharyngeal neuron and intestinal cells. How XRN2 affects molting is unknown, although this function may involve regulation of expression of MoLTing Defective 10 (MLT-10), another molting factor, in a direct or indirect manner, through an unknown mechanism. RNAi against *xrn-2* also causes slow growth and sterility (16), but again the basis of these phenotypes remains unknown.

To obtain a better understanding of the developmental functions of XRN2 and its role in miRNA turnover, we have characterized *xrn-2* null mutant *C. elegans*. We find that these animals arrest at the L2 stage, following a failed molt from the L1 to the L2 stage. The unanticipated ability to complete embryogenesis was not due to the absence of an essential embryonic function of XRN2, but reflected masking of the null phenotype due to maternal contribution. We demonstrate this through an *xrn-2ts* allele, which we generated by transplanting conditional mutations from yeast to *C. elegans*. We can thus show that XRN2 is essential during several stages of *C. elegans* development, including embryogenesis. These broader functions are consistent with a revised picture of *xrn-2* expression that we obtained using a rescuing transgene and detection of the endogenous protein by western blotting. Using small RNA deep sequencing to determine miRNA decay rates, we find that miR*s are generally less stable than miRs. Strikingly, among the small group of unstable miRs, only some become stabilized by inactivation of XRN2. We conclude that XRN2 has unanticipated miRNA substrate specificity *in vivo* and diverse developmental functions.

MATERIALS AND METHODS

Strains

Caenorhabditis elegans strains were cultured by standard methods described previously (24). The Bristol N2 strain was used as wild-type. Animals heterozygous for *xrn-2(tm3473)* were obtained from Dr Shohei Mitani, backcrossed three times and balanced. Strains used are shown in Supplementary Table S1.

Cloning and site-directed mutagenesis

Cloning and site-directed mutagenesis were performed by PfuUltra II Fusion HS DNA Polymerase (Agilent Technologies, Santa Clara, CA, USA) according to the supplier's protocol using specific primers (Supplementary Table S2). The codon-optimized *xrn-2* with three artificial introns (Supplementary Table S3) was designed according to a previous report (25) and synthesized using a commercial service (GenScript, Piscataway, NJ, USA).

Single-copy transgene insertion

DNA fragments were inserted into pCFJ210 (for chromosome I) or pCFJ201 (for chromosome IV) vectors by Multisite Gateway Technology (Life Technologies, Carlsbad, CA, USA) according to the supplier's protocol. Mos1-mediated single-copy transgene insertion was performed according to previous reports (26,27). Following confirmation of correct insertion by polymerase chain reaction (PCR), transgenic strains were backcrossed at least three times to the N2 strain.

Multicopy transgene arrays

The multisite gateway cloning system (Invitrogen) was used to insert transgenes into the pCG150 destination vector (containing *unc-119* rescuing fragment), which

was transformed into young adult *unc-119(ed3)* worms by microparticle bombardment using the Biolistic PDS-1000/He particle delivery system (BioRad) (28). For each bombardment, 16 µl of 0.5 µg/µl pCG150 and 4 µl of 0.8 µg/µl pCFJ90 (co-injection marker containing Pmyo-2::mCherry) were coupled to 1-µm microcarrier gold beads (BioRad, Cat#165-2263). Worms were allowed to recover for 1 h at 15°C after bombardment and were then grown at 25°C on NG 2% plates seeded with OP50 bacteria for ca. 2 weeks before screening for wild-type moving worms and mCherry-fluorescence from the co-injection marker. Transgenes containing wild-type or D234A-D236A double mutant *xrn-2* sequences were stably transmitted and expressed in the germline, suggesting integration into the genome.

Antibodies and western blotting

Recombinant full-length *C. elegans* XRN2 was prepared as described (16) and used to immunize rats (Charles River Laboratories, Kisslegg, Germany), to obtain an anti-XRN2 antibody. A mouse monoclonal anti-actin antibody (clone C4) was purchased from Millipore (Billerica, MA, USA). The anti-XRN2 antibody and anti-actin antibody were used with 1000- and 3000-fold dilutions, respectively, followed by horseradish peroxidase-conjugated secondary antibody (GE Healthcare, Little Chalfont, UK) reaction. The membranes were treated with ECL Western Blotting Detection Reagents, and protein bands were detected using Amersham Hyperfilm ECL (Figure 3C) or by an ImageQuant LAS 4000 hemiluminescence imager (all GE Healthcare) (Figure 4C). Band intensities were quantified using the ImageJ software (NIH, Bethesda, MD, USA).

Microscopy

Differential Interference Contrast (DIC) and fluorescent images were obtained using an Axio Observer Z1 microscope and AxioVision SE64 (release 4.8) software (Carl Zeiss, Oberkochen, Germany). Stereoscopic images were obtained by M205 A stereo microscope (Leica, Solms, Germany).

RNA preparation, sequencing and RT-qPCR

Gravid N2 or *xrn-2ts* worms were treated with bleaching solution [30% sodium hypochlorite (5% chlorine) reagent (Thermo Fisher Scientific, Waltham, MA, USA), 750 mM potassium hydroxide] to extract eggs, which were then incubated in M9 medium overnight to hatch. The resulting synchronized L1 larvae were cultured with *Escherichia coli* OP50 in S-medium supplemented with trace metal solution (29) at a concentration of 1×10^4 worms/ml with shaking (180 rpm) at 25°C for 2 h. Subsequently, α-amanitin (Sigma-Aldrich, St. Louis, MO, USA) was added to a final concentration of 50 µg/ml, which blocks transcription and stalls larval development (Supplementary Figure S2). A total of 1.5×10^4 worms were harvested at each sampling time point during the next 8 h, washed three times with M9 medium, resuspended in 700 µl of TRIzol reagent (Life Technologies) and frozen in liquid nitrogen. Worms were broken open by five repeats of freeze and thaw using liquid nitrogen and a 42°C heating block, before RNA was extracted and purified according to the supplier's protocol with the modification that RNA was incubated with 50% 2-propanol at −80°C overnight for efficient precipitation of small RNA.

Small RNA (15–30 nt) libraries were prepared from extracted total RNA using TruSeq Small RNA Sample Prep Kit (Illumina, San Diego, CA, USA) according to the supplier's protocol. All samples were multiplexed and 13 pM of the multiplexed libraries sequenced on two lanes of an Illumina HiSeq 2000 instrument using RTA 1.13.48. Individual reads were assigned to their sample based on the TruSeq barcode using the Illumina software Casava v1.8.0.

Quantification of individual miRNAs by reverse transcription-quantitative polymerase chain reaction (RT-qPCR) was done using TaqMan MicroRNA Assays (Life Technologies) and StepOnePlus Real-time PCR Systems (Applied Biosystems, Foster City, CA, USA) according to the suppliers' protocols. Forty nanogram of total RNA was used as a template for reverse transcription reaction (15 µl), and 1.3 µl of the reaction was used for qPCR reaction (25 µl). The miRNA levels were normalized to the small nucleolar RNA sn2841 levels.

For mRNA quantification, complementary DNA (cDNA) was generated from total RNA by ImProm-II Reverse Transcription System (Promega, Fitchburg, WI, USA) using oligo$(dT)_{15}$ primers (for Figure 4D) or random primers (for Supplementary Figure S2B, C) according to the supplier's protocol. RT-qPCR was performed with specific primers (Supplementary Table S2), a SYBR Green PCR Master Mix (Applied Biosystems) and a StepOnePlus Real-time PCR System. Primer sequences for pre-eft-3 mRNA and 18S ribosomal RNA were taken from (30) and (31), respectively.

Analysis of the miRNA sequencing data

For each read, the 3′ adaptor TGGAATTCTCGGGTGCCAAGG was removed by aligning it to the read allowing one or two mismatches in prefix alignments of at least 7 or 10 bases, respectively. Reads with low complexity were filtered out based on their dinucleotide entropy (removing <1% of the reads). Only reads with a minimum length of 14 nt were retained. Alignments to the miRNA database miRBase release 18 (http://www.mirbase.org/) were performed by the software bowtie (version 0.9.9.1) (32) with parameters -v 2 -a -m 100, tracking up to 100 best alignment positions per query and allowing at most two mismatches. Reads that mapped to a miRNA but at the same time also mapped with fewer mismatches to the genome (ce6) were filtered out. The expression of each miRNA was determined by counting the number of associated reads. To compensate for differences in the read depths of the individual libraries, each sample was divided by its total number of counts and multiplied by the average sample size. The resulting values were $\log_2$ transformed using a pseudo-count of 1 ($y = \log_2(x+1)$). To obtain relative decay rates for the time window t = 1 h to t = 8 h, the change in expression of

each miRNA over time was determined by the slope of a linear fit performed in R (www.r-project.org). Slopes for the two replicates were calculated separately and then averaged for further use.

Release 18 of miRBase does no longer provide identifiers that label a miRNA as a mature or a star form. We thus identified the star forms by firstly pairing the 5p and 3p forms using the miRNA name (without the −5p and −3p extensions) and then assigning the star label to the form with the lower expression level in the untreated sample.

Determination of miRNA half-life

We assumed miRNAs to decay exponentially according to the following equation:

$$N(t) = N_0 \cdot 2^{-t/\tau}$$

where t is the time, $N(t)$ is the concentration of the miRNA at time point t, N_0 is the starting concentration and τ is the half-life of the miRNA.

From this follows a linear relationship between the logarithmic concentration (measured as delta-Ct values) and the half-time τ:

$$log_2(N(t)) = (-1/\tau) \cdot t + log_2(N_0)$$

τ can be obtained from the slope of a linear regression by the following equation:

$$\tau = -1/slope$$

The intercept term captures differences in the starting concentration; for visualization, the term was subtracted from delta-Ct values.

The miRNA half-lives were calculated for individual replicate experiments. The half-life of stable miRNAs that decreased <20% (the detection limit) over the course of the 8-h experiment was set to 30 h, which is the τ resulting from a 20% decrease in 8 h and corresponds to a lower limit estimate for the half-life of such miRNAs.

The significance of differences in half-lives between worm strains was calculated using a two sample t-test assuming equal variances.

RESULTS

tm3473 is a *bona fide* null allele of *xrn-2*

Previous studies on *xrn-2* mutant phenotypes relied on its depletion by RNAi (16,22). However, knock-down of genes by RNAi is usually incomplete and may vary across tissues. Therefore, we set out to characterize the *xrn-2* mutant *xrn-2(tm3473)*, provided by Dr Shohei Mitani. The *tm3473*-allele is a deletion of 278 bases in exon 3 leading to a frame shift at amino acid position 278 and a premature stop codon at position 308 (Figure 1A). Western blotting using an antibody against XRN2 confirmed absence of full-length XRN2 protein in the *xrn-2(tm3473)* background (Figure 1B). This strain, and a wild-type strain included for comparison, contains a transgene to express full-length GFP-tagged XRN2 to achieve wild-type development (see later in the text). We also failed to detect a band corresponding to the predicted size of a potential truncated translation product (data not shown). Although we cannot formally exclude that the polyclonal antiserum that we used would fail to

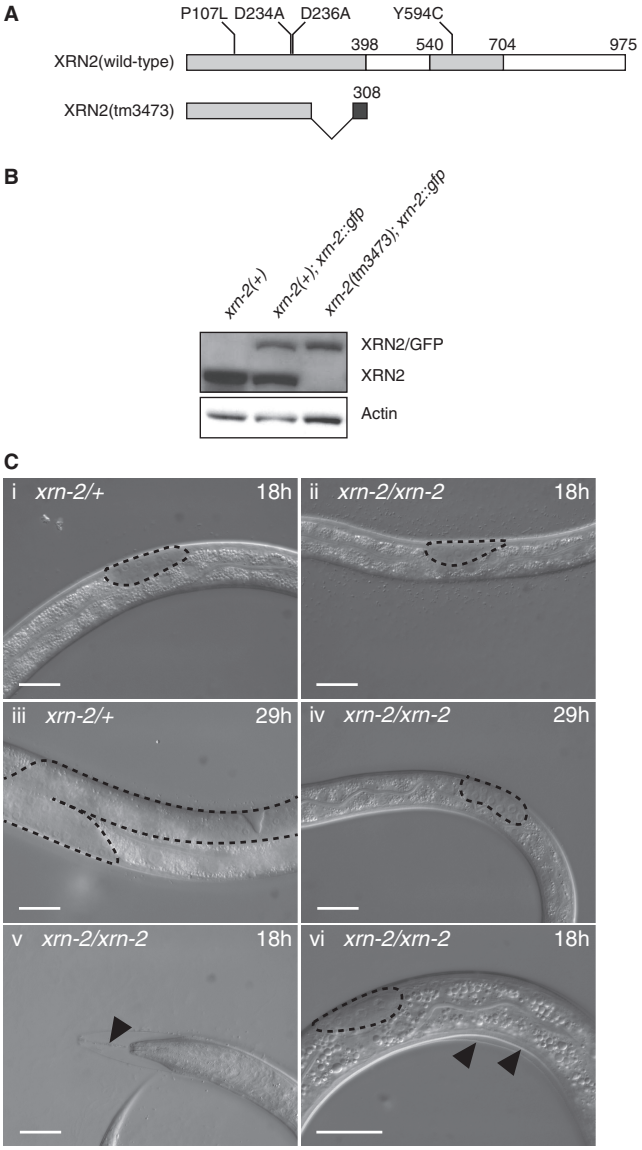

Figure 1. *xrn-2(tm3473)* is a *bona fide* null allele that causes molting defects and developmental arrest. (**A**) Schematic representation of wild-type and mutant XRN2. Conserved regions are shown in light grey. Dark grey indicates sequence unique to the *xrn-2(tm3473)* mutant due to a frame shift. Point mutations investigated in this study are indicated. (**B**) Western blotting confirms absence of endogenous XRN2 in the *xrn-2(tm3473)* background (lane 3). *xrn-2(+)* denotes the N2 wild-type strain. Note the presence of an XRN2/GFP-encoding transgene in the strains shown in lane 2 and 3, used to restore development of the *xrn-2(tm3473)* mutant strain. (**C**) DIC micrographs of worms grown at 25°C; gonads are outlined to facilitate staging. (i, ii) After 18 h, both *xrn-2*/+ (*tm3473* heterozygous) and *xrn-2*/*xrn-2* (*tm3473* homozygous) worms are at the L2 stage. (iii, iv) After 29 h, *xrn-2*/*xrn-2* worms remain arrested at the L2 stage (iv), whereas the heterozygous siblings have reached the L4 stage (iii). (v, vi) Larval arrest is accompanied by molting defects. *xrn-2*/*xrn-2* worms are unable to shed the pharyngeal cuticle (v, arrow head), which leads to superposition of the old and newly synthesized cuticle (vi, arrow heads). Scale bar, 20 μm.

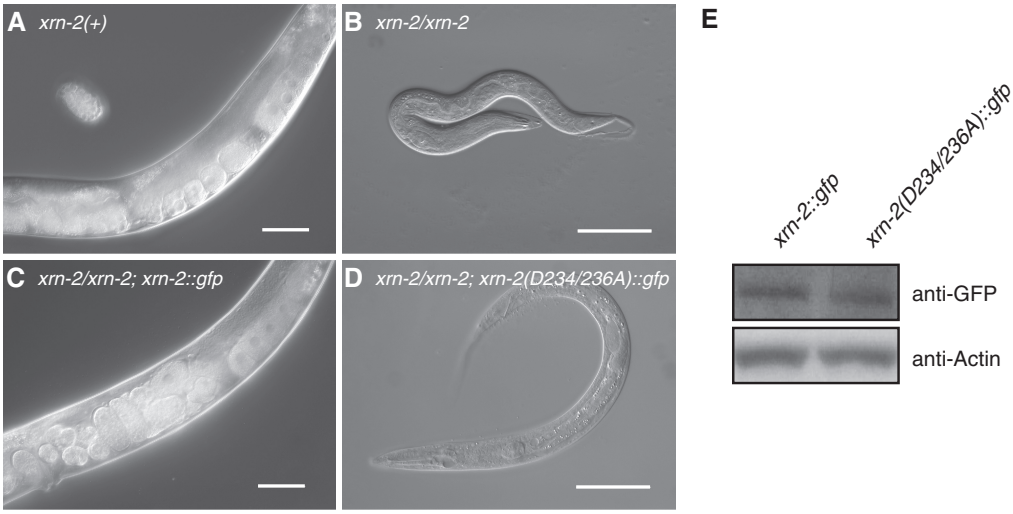

Figure 2. XRN2 catalytic activity is required for molting and growth beyond the L2 stage. (**A**) Wild-type worms develop into gravid adults, whereas (**B**) *xrn-2(tm3473)* homozygous worms arrest development. (**C**) Transgenic extrachromosomal *xrn-2* expressed under the control of the *xrn-2* 1413-bp promoter and *xrn-2* 3′-UTR rescues *xrn-2(tm3473)* mutant animals, whereas (**D**) a catalytically inactive version of *xrn-2* with two point mutations (D234A and D236A) does not. Both transgenes contain a C-terminal GFP tag, permitting their detection with an anti-GFP antibody. (E) Western blotting reveals equivalent accumulation of wild-type (lane 1) and mutant (lane 2) protein *in vivo*. Scale bar, 50 µm. *xrn-2(+)* denotes the N2 wild-type strain.

cross-react with such a truncated product despite the fact that it was raised against recombinant full-length protein, the data suggest that the mutant mRNA may be degraded through nonsense-mediated decay. We conclude that *xrn-2(tm3473)* is a bona fide null allele.

xrn-2(0) mutant animals fail to molt and arrest during L2

Worms exposed to *xrn-2(RNAi)* from L1 stage arrest as L4 larvae that are unable to ecdyse, i.e. shed the cuticle (22). By contrast, *xrn-2(tm3473)* animals already displayed penetrant defects in the L1-to-L2 molt (Figure 1C), the first molt during development. Ecdysis starts with loosening of the cuticle at the pharynx followed by rotations around the longitudinal axis that loosen the body cuticle (33). XRN2 appears to be involved in the early shedding of the cuticle taking place at the pharynx as the mouth of worms homozygous for *tm3473* remained attached to the old cuticle through a string-like structure [Figure 1C(v)]. The rest of the cuticle around the head and the body was at least partially detached [Figure 1C(v and vi)], and a new cuticle was already visible beneath the old one, indicating that XRN2 is predominantly involved in ecdysis rather than cuticle synthesis. Finally, following failure to shed the L1 cuticle, and possibly as a direct consequence (33), the mutant worms arrested during the L2 stage [Figure 1C(iv and iii)].

XRN-2 catalytic activity is required for molting

Although XRN2 is an RNase, it was not evident that the RNase activity was actually required for the developmental functions of this protein. XRN1 and XRN2 proteins share a conserved three amino acid motif, DXD, that is essential for exonuclease activity *in vivo* (11,34). The aspartic acids (D) in this motif are important for coordination of Mg^{2+} ions that are required for RNA hydrolysis. We thus constructed cDNA-based transgenes that encoded either the wild-type XRN2 or the catalytic dead D234A-D236A double mutant protein, where A stands for alanine. Both transgenes were driven from a promoter region covering 1.4 kb of upstream sequence and carried the *xrn-2* 3′-UTR as well as a C-terminal triple GFP/His_6/Flag-tag (Figure 2). As expected, the wild-type transgene efficiently rescued both the molting defect and larval arrest when introduced as a stable multicopy array (Figure 2C). By contrast, the mutant transgene was incapable of rescuing molting defect and larval arrest (Figure 2D), although mutant and wild-type protein accumulated at equivalent levels *in vivo* (Figure 2E). We conclude that the RNase activity of XRN2 is essential for its function in early larval development.

xrn-2 is expressed broadly and constitutively

Frand *et al.* (22) previously analysed the ability of a 132 bp sequence upstream from the *xrn-2* start codon to drive expression of *gfp* when present in a multicopy extrachromosomal array, and concluded that *xrn-2* expression was limited, occurring mostly in the pharyngeal myoepithelium, the intestine and certain neurons. This seemed surprising given that, based on our understanding of yeast and human Rat1p/XRN2 proteins, *C. elegans* XRN2 would be expected to be broadly involved in RNA processing and decay processes. Moreover, the Wormbase database annotates *xrn-2* as the second gene in a two-gene operon where rpl-43 is the upstream gene, 132 bp away (Figure 3A). In generating the rescuing transgene described earlier in the text, we had therefore used an extended sequence of 1413 bp upstream of the *xrn-2* start codon, reaching the 5'-end of the Y48B6A.1 ORF (Figure 3A). This construct revealed widespread, possibly ubiquitous expression, with XRN2/GFP signal

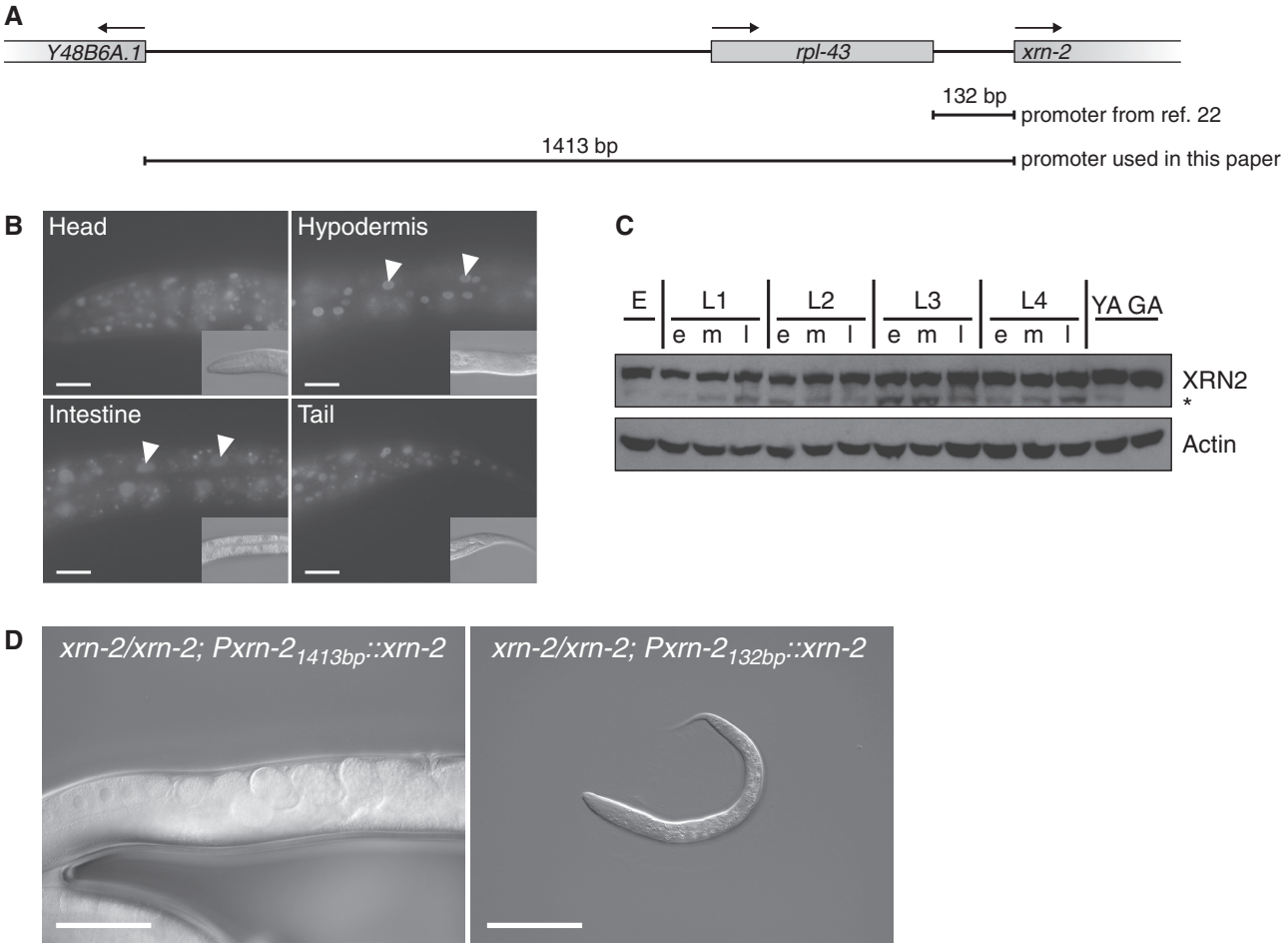

Figure 3. XRN2 is ubiquitously and constitutively expressed. (**A**) Schematic depiction of the *xrn-2* genomic locus and promoters used. The arrows indicate the direction of transcription. (**B**) Micrographs showing GFP signal of single-copy-integrated, codon-optimized and *gfp*-tagged *xrn-2* expressed under the control of the 1413-bp long promoter region. The GFP signal is ubiquitously detected. Examples of hypodermal and intestinal cells are marked with arrowheads. Insets: DIC images of the same worms. (**C**) Western blot showing a time-course for endogenous XRN2. 'e', 'm' and 'l' stands for early, mid and late, respectively; 'YA' and 'GA' for young and gravid adult, respectively. An asterisk indicates an apparent proteolytic fragment of XRN2, which did not occur consistently in other western blots. (**D**) Single-copy-integrated, codon-optimized and *gfp*-tagged *xrn-2* expressed under the control of the 1413-bp long *xrn-2* promoter region rescues the phenotypes of *xrn-2(tm3473)*, but the 132-bp long *xrn-2* promoter region does not. Scale bar, 20 μm (B) and 50 μm (D).

being detectable from early embryo through adulthood (Figure 3B). This expression was further validated through a time course that followed endogenous XRN2 protein by western blotting, and equally revealed continuous *xrn-2* expression throughout the *C. elegans* life cycle (Figure 3C).

Complementation of mutant phenotypes can provide a functional test for the authenticity of a putative promoter, and we found that *xrn-2* transgenes driven by the *xrn-2* 'long' promoter could rescue the *xrn-2(tm3473)* strain. This was true both when *xrn-2* cDNA was used (Figure 2C), which resulted in protein levels that were reduced relative to the endogenous protein (Figure 1B), and when a codon-optimized variant with synthetic introns was used (Figure 3D), which generated protein levels more similar to endogenous levels (see later in the text). By contrast, the *xrn-2* 'short' promoter failed to rescue the *xrn-2(tm3473)* mutation, although the optimized transgene was used (Figure 3D). Taken together, our results demonstrate that *xrn-2* is expressed broadly, perhaps ubiquitously, across tissues and developmental stages, and that expression beyond previously reported tissues is important for its role in molting.

A *xrn-2* temperature-sensitive allele generated *de novo* reveals additional XRN2 functions

Our finding of a molting defect as the predominant phenotype of *xrn-2* null mutant animals was consistent with a previously reported molting defect in *xrn-2(RNAi)* animals (22). However, given the broad expression of XRN2, which extends to the embryo, we wondered whether earlier phenotypes were obscured due to maternal contribution of mRNA or protein from *xrn-2*/+ heterozygous mothers to their *xrn-2*/*xrn-2* homozygous daughters. Rapidly inactivatable, conditional alleles would permit addressing this issue, but such alleles can currently not be generated in a targeted manner, for a specific gene of interest, in *C. elegans*. However, temperature-sensitive (ts) alleles have been described in *Saccharomyces cerevisiae* for Rat1p (35) and the Rat1p/XRN2 paralogue Xrn1p

(36). Individual mutation of either aspartate of the DXD motif mentioned earlier in the text to alanine (A) may further impair but not abrogate Mg^{2+} binding and render the protein function ts (34). We thus went to test whether the corresponding mutations in *C. elegans xrn-2*-elicited temperature sensitivity within the worm's physiological temperature window, ~10°C below that of yeast. We introduced single-copy integrated *xrn-2* transgenes with appropriate mutations into strains that were homozygous for *xrn-2(tm3473)*, i.e. lacked endogenous XRN2. Among three distinct mutations that we tested (Figure 1A), P107L, corresponding to *S. cerevisiae xrn1-10(P90L)* (36), conferred temperature sensitivity, supporting viability at 15°C but not at 25°C. By contrast, a Y594C-mutant transgene supported viability at either temperature, whereas the D234A mutant transgene rescued at neither temperature. In the following, we will refer to the mutant strain that expresses *xrn-2P107L* as $xrn\text{-}2ts_{cDNA}$ to distinguish it from an optimized version described later in the text. An analysis of different temperature regimens revealed numerous phenotypes of $xrn\text{-}2ts_{cDNA}$ animals beyond the molting defect observed with the *xrn-2* null strain, including arrest in embryonic development and sterility (Supplementary Figure S1). These mutant strains thus revealed multiple functions of XRN2 beyond molting, which had been obscured in the null mutant animals.

Although the $xrn\text{-}2ts_{cDNA}$ transgene permitted rapid and tight inactivation of *xrn-2* (Supplementary Figure S1), it failed to provide full XRN2 activity at the permissive temperature as illustrated by slow growth and small brood sizes small (~25 relative to ~250 for wild-type animals) relative to wild-type animals. This reduced the strain's utility for molecular or biochemical studies or genetic screens. Because low-protein levels relative to the endogenous protein (Figure 1B) might account for the reduced functionality, we introduced artificial introns into the *xrn-2* cDNA and optimized its codon composition (25). For the wild-type protein, these nucleotide changes increased XRN2/GFP levels as determined by epifluorescence microscopy (data not shown). Moreover, *xrn-2(tm3473)* animals expressing the sequence-optimized xrn-2P107L::*gfp* single-copy transgene, which we will henceforth call *xrn-2ts*, grew better (although still more slowly than wild-type animals) and had an increased brood size. At the same time, we could still rapidly and efficiently inactivate the optimized transgene by raising the temperature (Figure 4A, B), although a fully penetrant embryonic or L1 arrest now necessitated incubation at 26°C, rather than 25°C. Viability and development of N2 wild-type animals remained unimpaired at this temperature (Figure 4B) (37).

The P107L mutation induces temperature sensitivity by reducing XRN2 stability

To test whether destabilization of the protein by elevated temperature contributed to the ts behavior of *xrn-2P107L*, we examined steady-state levels of XRN2 at 15 and 26°C. We observed that XRN2 levels were substantially lower in the *xrn-2ts* mutant strain than either N2 or a strain carrying the wild-type transgene (Figure 4C). We note that wild-type XRN2/GFP levels were also reduced relative to endogenous XRN2 concentration in N2, particularly at 26°C, but the decrease was less than that seen with XRN2P107L/GFP. Hence, it seems likely that the P107L mutation renders XRN2 ts by destabilizing it, consistent also with its location directly adjacent to an unusually long α-helix, previously termed 'tower domain' (11). To test this possibility further, we quantified *xrn-2* mRNA levels in the two *xrn-2* transgenic strains. Unlike XRN2 protein levels, the *xrn-2* mRNA levels were not reduced in the mutant strain. In fact, *xrn-2ts* mRNA accumulated at increased concentrations relative to the wild-type mRNA, particularly at 26°C (Figure 4D). Hence, these results not only confirm that the P107L mutation causes temperature sensitivity by reducing XRN2 protein stability but also indicate the existence of an auto-regulatory mechanism that promotes transcription or stabilization of *xrn-2* mRNA when XRN2 activity is low.

The miR* strands decay more rapidly than guide strands

Our previous studies (16,38) had implicated *C. elegans* XRN2 in miRNA turnover by revealing increased steady-state levels of certain endogenous miRNAs in *xrn-2(RNAi)* worms and XRN2-dependent degradation of naked or Argonaute-loaded miRNAs in worm lysates. However, a formal demonstration that XRN2 depletion slowed miRNA degradation *in vivo* was missing. Moreover, certain endogenous miRNAs appeared unchanged on XRN2 depletion, but whether due to substrate specificity, or technical limitations, e.g. in the kinetics or tissue distribution of RNAi-mediated XRN2 depletion, remained unknown. To address these two issues, we examined miRNA decay globally *in vivo* in wild-type N2 animals. We performed a time-course experiment in which we inhibited transcription in L1 stage larvae by addition of α-amanitin (Supplementary Figure S2) and surveyed miRNAs at several subsequent time points over the next 8 h by deep sequencing (Figure 5A). We chose the L1 stage because these larvae had previously been reported to be sensitive to treatment with α-amanitin (39), and we confirmed that this treatment efficiently blocked transcription by assaying eft-3 pre-mRNA levels (Supplementary Figure S2B, C). For each time point, we calculated the levels of each miRNA as reads normalized to average library size ('Materials and Methods' section), which means that these numbers can go up or down or stay unchanged for a given miRNA depending on whether it decays less rapidly, more rapidly or just as rapidly as the average miRNA in this pool. Accordingly, the fold changes per hour in $\log_2$ can be positive, negative or 0, with negative values indicating less stable miRNAs. However, these values cannot be translated into absolute decay rates.

The fold changes per hour thus calculated for two independent biological replicates correlated well (Supplementary Figure S3) and their averages were used for subsequent analysis. A scatter plot displaying fold changes versus read numbers revealed that decay rates were broadly distributed with a subset of miRNAs displaying a strikingly faster decay than average (Figure

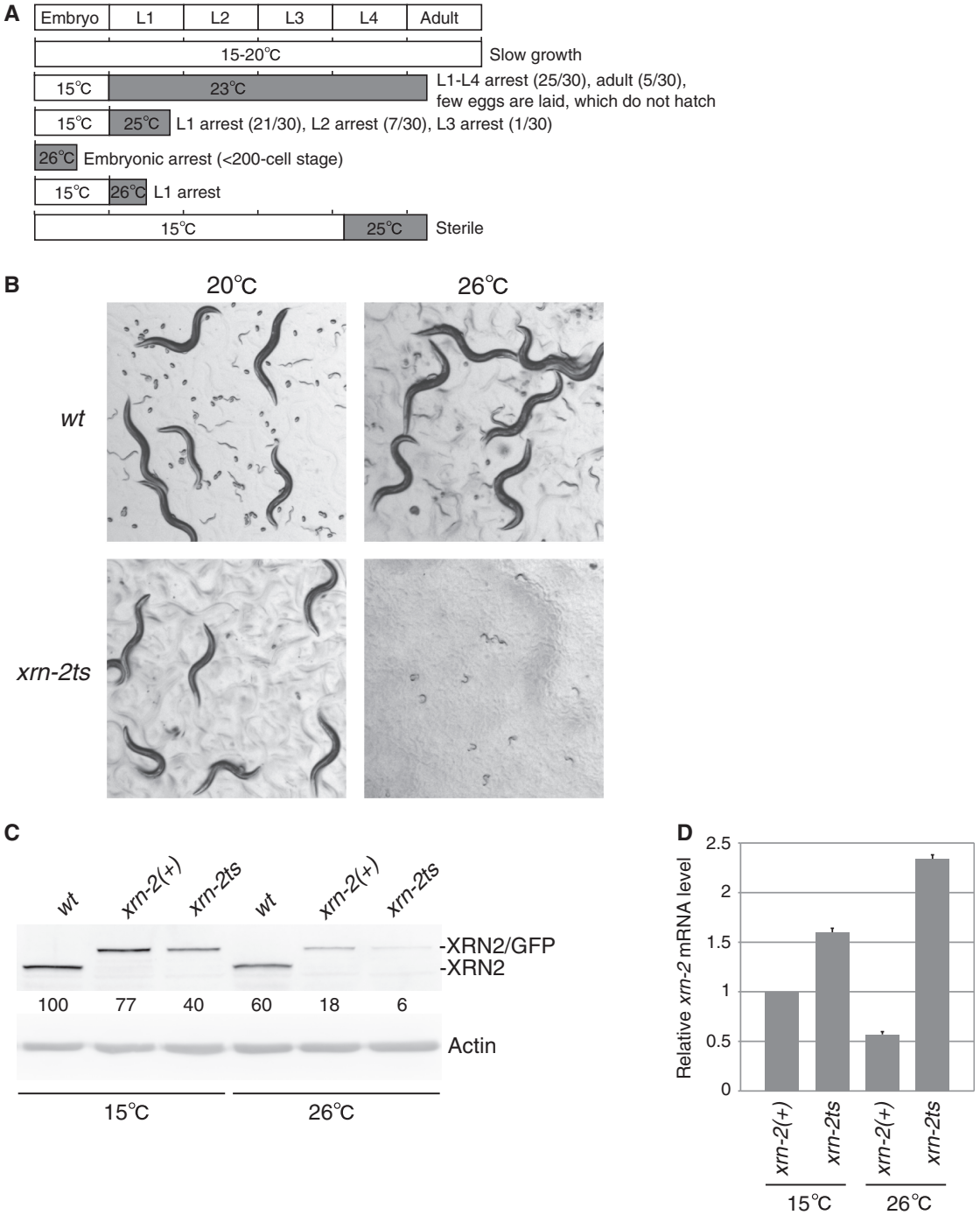

Figure 4. Characterization of an improved *xrn-2ts* strain reveals reduced XRN2 levels at restrictive temperature. (**A**) Schematic representation of *xrn-2ts* phenotypes at different temperature. *xrn-2ts* embryos or worms were cultured under the indicated conditions. Phenotypes observed are described on the right. For less-penetrant phenotypes, a number indicating worms affected/worms scored is shown in brackets. (**B**) The wild-type ('wt'; N2) and *xrn-2ts* worms were cultured from L1-stage at 20 or 26°C as indicated for 72 h (wt) and 93 h (*xrn-2ts*), respectively. The worms were observed by stereo microscopy at the same magnification. (**C, D**) The wt, *xrn-2(+)* and *xrn-2ts* worms were cultured from mid L3- to late L4-stage at 15°C or 26°C and harvested. (C) XRN2, XRN2/GFP and actin protein levels were examined by western blotting. XRN2 and XRN2/GFP levels were normalized to actin levels and shown with values of wt at 15°C defined as 100. (D) The mRNA levels of the *xrn-2::gfp* transgenes in *xrn-2(+)* and *xrn-2ts* worms were quantified by RT-qPCR, normalized to actin mRNA levels and shown with values of *xrn-2(+)* at 15°C as 1 ($n = 2$, means + SEM). '*xrn-2(+)*' denotes *xrn-2(tm3473)* homozygous animals expressing a wild-type *xrn-2* transgene.

5B). The effect was particularly pronounced for miRNAs of lower abundance. Strikingly, when we coloured miR*s, operationally defined as the one of two miRNA strands derived from a pre-miRNA that is less abundant, in red, and miRs in black, a clear separation of colours became apparent (Figure 5B). Hence, highly unstable RNAs were almost exclusively miR*s (Figure 5B). This result makes immediate and intuitive sense when considering miR*s as

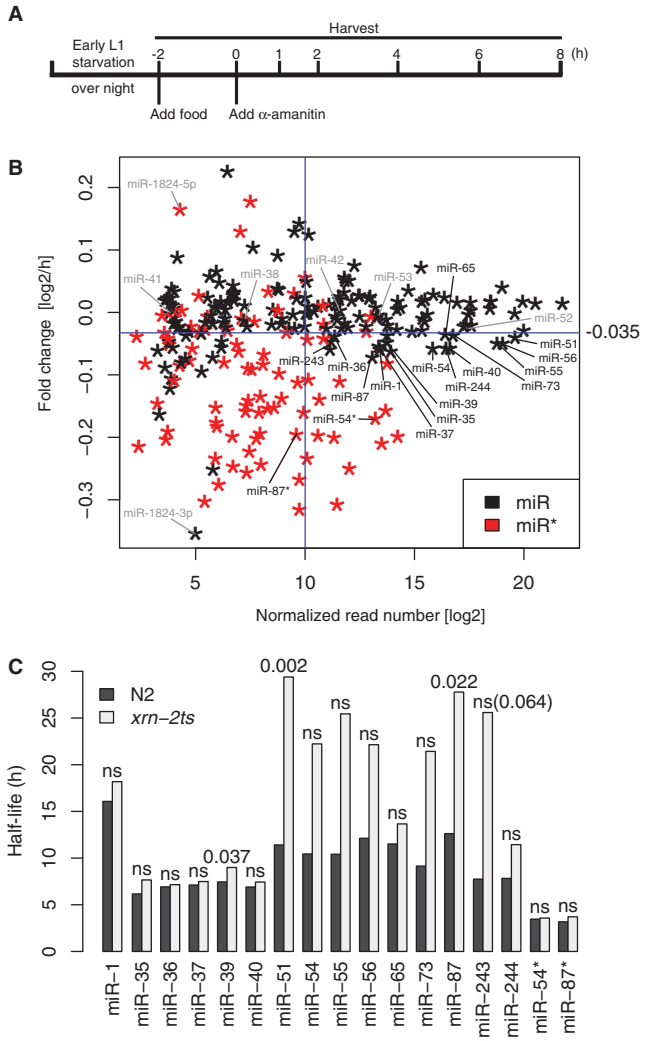

Figure 5. Specific miRNAs are stabilized on XRN2 depletion. (**A**) Experimental design for miRNA decay analysis. RNA was extracted for (**B**) deep sequencing and (**C**) RT-qPCR analyses. (B) Relative decay rates of miRNAs are plotted against normalized reads for miRNAs with sufficient expression ('Materials and Methods' section). Black stars, miRs; red stars, miR*s. Fifteen miRs that showed high-read numbers and fast relative decay as indicated by the blue cut-off lines. (Because the plot shows fold changes per hour, not decay constants, unstable miRNAs are those below the cut-off line.) These and two miR*s, indicated in black, were further examined by RT-qPCR. Other miRs discussed in the main text are shown in grey. (C) The miRNA levels at each time point in wt and *xrn-2ts* worms were quantified by RT-qPCR, and their half-lives were calculated as described in 'Materials and Methods' section. Relevant *P*-values are shown. ns, not significant.

biogenesis byproducts. It is also consistent with generally long miRNA half-lives observed in a microarray-based study that was confined to a survey of annotated miRs (40).

Specific miRNAs are stabilized on XRN2 inactivation

Although the fast decay rates were preferentially seen for miR*s, some miRs exhibited unusually low stability, most notably several members, though not all, of each of the miR-35 (miR-35 through miR-42) and the miR-51 (miR-51 through miR-56) families. To test whether this was due to decay by XRN2, we repeated the α-amanitin time-course experiment for wild-type and *xrn-2ts* worms. Under the conditions that we use, α-amanitin completely blocks development at the early L1 stage (Supplementary Figure S2; Supplementary Materials and Methods), so that wild-type and *xrn-2ts* animals are equally arrested in development.

For this analysis, we focused on miRNAs with low stability (apparent $\log_2$ fold change of less than −0.035/h and thus below the blue cut-off line in Figure 5B) and moderately high, to high, expression levels ($>2^{10}$ normalized reads, to the right of the cut-off line). We determined the levels of individual miRNAs by RT-qPCR and normalized them to sn2841, a small nucleolar RNA whose level is stable during the time course (data not shown). When testing the five rapidly decaying members of the miR-35 family, all of them displayed comparable half-lives in wild-type and *xrn-2ts* animals (Figure 5C and Supplementary Figure S4). Similarly, *xrn-2* inactivation had little effect on the decay of miR-1, miR-65 and miR-244. By contrast, the decay of miR-51 and miR-87 was substantially and significantly delayed in *xrn-2ts* animals. The miR-54, miR-55, miR-56, miR-73 and miR-243 showed a similar trend, although differences failed to reach statistical significance (Supplementary Figure S4). We also examined decay of the highly expressed and unstable miR-54* and found it to be unaffected by XRN2 inactivation. Similarly, miR-87*, unlike miR-87, continued to decay rapidly when XRN2 was inactive. As the passenger and guide strand derive from the same precursor, this directly confirms that the decreased apparent half-lives of the guide strands truly reflects stabilization of this guide strand and not a secondary effect of altered processing of residual pre-miRNAs. Taken together, our data reveal that XRN2 is essential for rapid decay of a subset of miRNAs during the first larval stage.

DISCUSSION

xrn-2 is broadly expressed and functions in processes beyond molting

Although molecular functions of XRN2 proteins have been studied extensively, particularly in yeast and cultured human cells, their developmental functions have remained virtually unexplored (15). An RNAi-based screen had implicated XRN2 in molting in *C. elegans*, consistent also with its expression in tissues important for cuticle generation or shedding (22), and in agreement with this idea, we find that an *xrn-2* null mutation causes a penetrant L1 molting defect and subsequent L2 stage arrest. However, by generating a conditional allele, we could demonstrate that this only represents the tip of the iceberg; XRN2 in *C. elegans* is required for numerous events during embryonic and post-embryonic development as demonstrated for instance by embryonic lethality and sterility under appropriate regimens.

In yeast, where Rat1p/XRN2 is essential for viability, mutations cause a diverse array of defects in various RNA

metabolic processes, such as transcriptional termination, ribosomal RNA processing, intron degradation and aberrant transfer RNA degradation (15). However, it remains to be determined which of these processes constitutes the essential function of Rat1p or whether it is any one process. Similarly, it remains to be established for *C. elegans* whether the requirements for functional XRN2 in different tissues and developmental stages reflect a core underlying theme, or whether the respective targets and processes that become dysregulated on XRN2 depletion vary. We also note that although we have focused here on miRNAs as the only currently known substrate of *C. elegans* XRN2, it is highly likely that numerous additional substrates exist, and any of these, individually or in combination, may be relevant for the *xrn-2* mutant phenotypes. Nonetheless, our demonstration that mutations inactivating the XRN2 catalytic site also abrogate its ability to complement an *xrn-2* null mutation argue that it is processing or degradation of one or several RNA substrates that are important for the function of XRN2 in molting. Modulator, i.e. enhancer and suppressor, screens may offer a way forward to identify specific targets and pathways affected by *xrn-2* deficiency and have been initiated in our laboratory.

XRN2 substrate preferences

In vitro, XRN2 proteins can degrade various RNA sequences, provided they are 5′-monophosphorylated and devoid of stable structures (9,10). However, we find here that in the L1 stage, only a subset of miRNAs is stabilized on XRN2 inactivation. We cannot formally rule out that XRN2 activity at the restrictive temperature is not fully eliminated in the *xrn-2ts* strain and that complete loss of activity would stabilize all miRNAs. Nonetheless, the available data demonstrate that, minimally, some miRNAs are more dependent on XRN2 for degradation than others.

The mechanisms that provide specificity remain to be elucidated. On the XRN2 side, the enzyme may either contain previously unrecognized intrinsic specificity, or its substrate range may be restricted specifically *in vivo* through the action of protein binding partners, such as the newly identified PAXT-1 (41). Similarly, features of the miRNA that render them sensitive or insensitive to XRN2 remain to be identified. Although we lack enough examples of miRNAs that are stabilized by mutation of *xrn-2* to confidently comment on the involvement of sequence features, we note that there is almost no overlap in sequence between miR-51 and miR-87, and they even differ in their 5' ends, with miR-51 sporting the miRNA-characteristic U and miR-87 and miR-243 a more unusual G and C, respectively. Hence, it seems possible that instead of, or in addition to, sequence, the site of expression of an miRNA might affect its sensitivity to degradation by XRN2. Because our expression analysis of XRN2 indicates widespread, possibly ubiquitous expression of *xrn-2*, such a model would imply the existence of additional factors that either promote degradation of specific miRNAs by XRN2 in some tissues or prevent it in others. Targets of miRNAs might be one such factor. We previously reported that target RNAs protected their cognate miRNAs from degradation (16,38). At this point, it is not known whether any target can do this, for any miRNA, or if specific miRNA-target duplex architectures are required. Nonetheless, differences in the levels of either the entire group of target RNAs, or only individual targets, might thus alter XRN2 activity towards miRNAs in a tissue-specific manner.

Finally, intracellular localization of miRNAs may affect their susceptibility to degradation by XRN2. This notion is based on our finding that XRN2 accumulates preferentially, perhaps exclusively in the nucleus [this study and (42)]. By contrast, miRNAs are thought to function in the cytoplasm, where they would thus be shielded from XRN2 activity. At the same time, a number of mature *C. elegans* miRNAs have recently been detected in both nucleus and cytoplasm, with individual miRNAs apparently differing in their nucleocytoplasmic distribution (43). However, because we have so far been unable to achieve sufficiently clean fractionation of nuclei versus cytoplasm, it remains to be determined whether XRN2-sensitive miRNAs partition more extensively to the nucleus than those that are XRN2-insensitive.

miRs and miR*s differ in their stabilities

Initially, it was assumed that miRNA precursors give rise to only one functional molecule, the mature miRNA or guide strand/miR. A second partially complementary molecule derived from the opposite strand of the pre-miRNA, the passenger strand/miR*, might be visible at much lower levels and constitute merely a biogenesis intermediate. More recently, however, several examples of functional miR*s have been described, and it has emerged that in some cases the ratio of miR to miR* may be variable and change with site of expression or development (18). Accordingly, a different nomenclature that identifies miRNA molecules based on their provenance from either the 5′ or the 3′ arm of the pre-miRNA has been adopted. Although there can be little doubt on the functionality of certain miR*s, our decay data strongly suggest that at least in our system most of them accumulate only transiently, supporting their designation as processing intermediates. Although ours is the first demonstration of this phenomenon on a global scale, Winter and Diederichs previously examined the half-lives of a small number of miRs and miR*s in human cells and equally observed reduced half-lives of the latter (44). Moreover, they noted that over-expression of Argonaute proteins could stabilize two miR*s that were investigated, suggesting that it is lack of Argonaute loading that renders miR*s unstable, which would also deprive them of a functional miRNA status.

We note that the least stable of all miRNAs that we observe is annotated as miR, miR-1824-3p, rather than miR*. However, deep sequencing is subject to sequence-dependent biases that prevent exact quantification of distinct small RNAs [(45) and our unpublished data]. The miR-1824-3p displays only marginally (~1.6-fold) more reads than its presumed miR*, miR-1824-5p,

which is much more stable ($\log_2$ fold change of 0.16/h versus −0.35/h for 5p versus 3p). Hence, we predict that absolute quantification would reveal that miR-1824-5p is more abundant than miR-1824-3p and thus the true miR by our criterion.

De novo generation of a conditional *xrn-2* allele

Genetic mutations are invaluable tools in assigning function to genes. However, if a gene has multiple consecutive functions in development, it can be difficult or impossible to study all of them with 'constitutive' mutations especially when an early function is essential during development. At the same time, for essential genes, homozygously mutant animals by necessity need to be derived from heterozygous parents, which may contribute mRNA or protein to their offspring so that early phenotypes can be masked (46). RNAi may be used to deplete such maternal mRNAs, but usually results in only partial depletion of transcripts and protein products. Similarly, although RNAi may be applied such that an early terminal phenotype in development is bypassed (47,48), it can usually not be timed precisely. Although *xrn-2(RNAi)* phenocopies the sterile phenotype of *xrn-2ts* animals, none of the conditions we tried so far were able to elicit embryonic lethality.

Conditional alleles, encoding rapidly inactivatable gene products, would permit addressing both of the aforementioned issues. The ts alleles are widely used for instance in yeast, and screens have been conducted in *C. elegans* to identify ts alleles for specific processes. However, because it has not been possible to predict a priori which mutations will generate a ts allele, targeted approaches for generation of conditional alleles of specific genes have been lacking.

We provide here proof of principle that a *C. elegans* ts mutation can be generated *de novo* by exploiting information from a different organism, yeast, despite major differences in their physiological temperature ranges. We note that our approach is not easily scalable and its generality remains to be established. However, many yeast ts alleles exist, and new ones can easily be generated, e.g. by complementing yeast deletion mutant cells with randomly mutagenized transgenes expressing the genes of interests. Hence, ours may be a fertile approach for other researchers interested in generating conditionally mutant *C. elegans* strains, complementing transcriptional (49,50), co-transcriptional (51) or post-transcriptional (52) approaches that modulate mRNA levels and thus, indirectly, protein activity.

ACCESSION NUMBERS

The small RNA sequencing data discussed in this study have been deposited at GEO and can be accessed at http://www.ncbi.nlm.nih.gov/geo/query/acc.cgi?token=xdwvjqcwsguaozo&acc=GSE46753.

SUPPLEMENTARY DATA

Supplementary Data are available at NAR Online.

ACKNOWLEDGEMENTS

The authors are grateful to Dr Iskra Katic, Dr Rafal Ciosk and Matyas Ecsedi for helpful comments on the manuscript. The authors thank Kirsten Jacobeit and Sophie Dessus-Babus of the FMI Functional Genomics Facility for library preparation and sequencing, which was performed at the Basel Deep Sequencing Facility, Dr Iskra Katic for help with *C. elegans* transgenesis and Dr David T. Harris and Dr Robert H. Horvitz for strain MT16418. The authors are particularly grateful to Dr Shohei Mitani and the National Bioresource Project for *C. elegans* (Japan) for the *tm3473* allele, and to Dr Saibal Chatterjee for generating XRN2 protein used to raise the anti-XRN2 antibody.

FUNDING

European Union Seventh Framework Programme (FP7/2007-2013) under grant agreement number [241985] (European Research Council 'miRTurn'). Novartis Research Foundation through the FMI and the Swiss National Science Foundation [SNF 31003A_127052 and SNF 31003A_143313]. Boehringer Ingelheim Fonds PhD fellowship (to S.R.). Funding for open access charge: European Union Seventh Framework Programme.

Conflict of interest statement. None declared.

REFERENCES

1. Miki,T.S. and Großhans,H. (2013) The multifunctional RNase XRN2. *Biochem. Soc. Trans.*, **41**, 825–830.
2. Henry,Y., Wood,H., Morrissey,J.P., Petfalski,E., Kearsey,S. and Tollervey,D. (1994) The 5′ end of yeast 5.8S rRNA is generated by exonucleases from an upstream cleavage site. *EMBO J.*, **13**, 2452–2463.
3. Petfalski,E., Dandekar,T., Henry,Y. and Tollervey,D. (1998) Processing of the precursors to small nucleolar RNAs and rRNAs requires common components. *Mol. Cell. Biol.*, **18**, 1181–1189.
4. Villa,T., Ceradini,F., Presutti,C. and Bozzoni,I. (1998) Processing of the intron-encoded U18 small nucleolar RNA in the yeast *Saccharomyces cerevisiae* relies on both exo- and endonucleolytic activities. *Mol. Cell. Biol.*, **18**, 3376–3383.
5. Qu,L.H., Henras,A., Lu,Y.J., Zhou,H., Zhou,W.X., Zhu,Y.Q., Zhao,J., Henry,Y., Caizergues-Ferrer,M. and Bachellerie,J.P. (1999) Seven novel methylation guide small nucleolar RNAs are processed from a common polycistronic transcript by Rat1p and RNase III in yeast. *Mol. Cell. Biol.*, **19**, 1144–1158.
6. Geerlings,T.H., Vos,J.C. and Raue,H.A. (2000) The final step in the formation of 25S rRNA in *Saccharomyces cerevisiae* is performed by 5′–>3′ exonucleases. *RNA*, **6**, 1698–1703.
7. Kim,M., Krogan,N.J., Vasiljeva,L., Rando,O.J., Nedea,E., Greenblatt,J.F. and Buratowski,S. (2004) The yeast Rat1 exonuclease promotes transcription termination by RNA polymerase II. *Nature*, **432**, 517–522.
8. Chernyakov,I., Whipple,J.M., Kotelawala,L., Grayhack,E.J. and Phizicky,E.M. (2008) Degradation of several hypomodified mature tRNA species in *Saccharomyces cerevisiae* is mediated by Met22 and the 5′-3′ exonucleases Rat1 and Xrn1. *Genes Dev.*, **22**, 1369–1380.
9. Kenna,M., Stevens,A., McCammon,M. and Douglas,M.G. (1993) An essential yeast gene with homology to the exonuclease-encoding XRN1/KEM1 gene also encodes a protein with exoribonuclease activity. *Mol. Cell. Biol.*, **13**, 341–350.
10. Stevens,A. and Poole,T.L. (1995) 5′-exonuclease-2 of *Saccharomyces cerevisiae*. Purification and features of ribonuclease

activity with comparison to 5′-exonuclease-1. *J. Biol. Chem.*, **270**, 16063–16069.
11. Xiang,S., Cooper-Morgan,A., Jiao,X., Kiledjian,M., Manley,J.L. and Tong,L. (2009) Structure and function of the 5′–>3′ exoribonuclease Rat1 and its activating partner Rai1. *Nature*, **458**, 784–788.
12. Heyer,W.D., Johnson,A.W., Reinhart,U. and Kolodner,R.D. (1995) Regulation and intracellular localization of *Saccharomyces cerevisiae* strand exchange protein 1 (Sep1/Xrn1/Kem1), a multifunctional exonuclease. *Mol. Cell. Biol.*, **15**, 2728–2736.
13. Hsu,C.L. and Stevens,A. (1993) Yeast cells lacking 5′–>3′ exoribonuclease 1 contain mRNA species that are poly(A) deficient and partially lack the 5' cap structure. *Mol. Cell. Biol.*, **13**, 4826–4835.
14. Johnson,A.W. (1997) Rat1p and Xrn1p are functionally interchangeable exoribonucleases that are restricted to and required in the nucleus and cytoplasm, respectively. *Mol. Cell. Biol.*, **17**, 6122–6130.
15. Nagarajan,V.K., Jones,C.I., Newbury,S.F. and Green,P.J. (2013) XRN 5'–>3' exoribonucleases: Structure, mechanisms and functions. *Biochim. Biophys. Acta*, **1829**, 590–603.
16. Chatterjee,S. and Großhans,H. (2009) Active turnover modulates mature microRNA activity in *Caenorhabditis elegans*. *Nature*, **461**, 546–549.
17. Krol,J., Loedige,I. and Filipowicz,W. (2010) The widespread regulation of microRNA biogenesis, function and decay. *Nat. Rev. Genet.*, **11**, 597–610.
18. Mah,S.M., Buske,C., Humphries,R.K. and Kuchenbauer,F. (2010) miRNA*: a passenger stranded in RNA-induced silencing complex? *Crit. Rev. Eukaryot. Gene Expr.*, **20**, 141–148.
19. Fabian,M.R. and Sonenberg,N. (2012) The mechanics of miRNA-mediated gene silencing: a look under the hood of miRISC. *Nat. Struct. Mol. Biol.*, **19**, 586–593.
20. Mendell,J.T. and Olson,E.N. (2012) MicroRNAs in stress signaling and human disease. *Cell*, **148**, 1172–1187.
21. Lu,Y., Liu,P., James,M., Vikis,H.G., Liu,H., Wen,W., Franklin,A. and You,M. (2010) Genetic variants cis-regulating Xrn2 expression contribute to the risk of spontaneous lung tumor. *Oncogene*, **29**, 1041–1049.
22. Frand,A.R., Russel,S. and Ruvkun,G. (2005) Functional genomic analysis of *C. elegans* molting. *PLoS Biol.*, **3**, e312.
23. Johnstone,I.L. (2000) Cuticle collagen genes. Expression in *Caenorhabditis elegans*. *Trends Genet.*, **16**, 21–27.
24. Brenner,S. (1974) The genetics of *Caenorhabditis elegans*. *Genetics*, **77**, 71–94.
25. Redemann,S., Schloissnig,S., Ernst,S., Pozniakowsky,A., Ayloo,S., Hyman,A.A. and Bringmann,H. (2011) Codon adaptation-based control of protein expression in *C. elegans*. *Nat. Methods*, **8**, 250–252.
26. Frokjaer-Jensen,C., Davis,M.W., Hopkins,C.E., Newman,B.J., Thummel,J.M., Olesen,S.P., Grunnet,M. and Jorgensen,E.M. (2008) Single-copy insertion of transgenes in *Caenorhabditis elegans*. *Nat. Genet.*, **40**, 1375–1383.
27. Frokjaer-Jensen,C., Davis,M.W., Hollopeter,G., Taylor,J., Harris,T.W., Nix,P., Lofgren,R., Prestgard-Duke,M., Bastiani,M., Moerman,D.G. *et al.* (2010) Targeted gene deletions in *C. elegans* using transposon excision. *Nat. Methods*, **7**, 451–453.
28. Praitis,V., Casey,E., Collar,D. and Austin,J. (2001) Creation of low-copy integrated transgenic lines in *Caenorhabditis elegans*. *Genetics*, **157**, 1217–1226.
29. Lewis,J.A. and Fleming,J.T. (1995) Basic culture methods. *Methods Cell Biol.*, **48**, 3–29.
30. Guang,S., Bochner,A.F., Burkhart,K.B., Burton,N., Pavelec,D.M. and Kennedy,S. (2010) Small regulatory RNAs inhibit RNA polymerase II during the elongation phase of transcription. *Nature*, **465**, 1097–1101.
31. Sumitani,M., Kasashima,K., Matsugi,J. and Endo,H. (2011) Biochemical properties of *Caenorhabditis elegans* HMG-5, a regulator of mitochondrial DNA. *J. Biochem.*, **149**, 581–589.
32. Langmead,B., Trapnell,C., Pop,M. and Salzberg,S.L. (2009) Ultrafast and memory-efficient alignment of short DNA sequences to the human genome. *Genome Biol.*, **10**, R25.
33. Singh,R.N. and Sulston,J.E. (1978) Some observations on molting in *Caenorhabditis elegans*. *Nematologica*, **24**, 63–71.
34. Solinger,J.A., Pascolini,D. and Heyer,W.D. (1999) Active-site mutations in the Xrn1p exoribonuclease of *Saccharomyces cerevisiae* reveal a specific role in meiosis. *Mol. Cell. Biol.*, **19**, 5930–5942.
35. Amberg,D.C., Goldstein,A.L. and Cole,C.N. (1992) Isolation and characterization of RAT1: an essential gene of *Saccharomyces cerevisiae* required for the efficient nucleocytoplasmic trafficking of mRNA. *Genes Dev.*, **6**, 1173–1189.
36. Page,A.M., Davis,K., Molineux,C., Kolodner,R.D. and Johnson,A.W. (1998) Mutational analysis of exoribonuclease I from *Saccharomyces cerevisiae*. *Nucleic Acids Res.*, **26**, 3707–3716.
37. Alvarez-Saavedra,E. and Horvitz,H.R. (2010) Many families of *C. elegans* microRNAs are not essential for development or viability. *Curr. Biol.*, **20**, 367–373.
38. Chatterjee,S., Fasler,M., Bussing,I. and Großhans,H. (2011) Target-mediated protection of endogenous microRNAs in *C. elegans*. *Dev. Cell*, **20**, 388–396.
39. Sanford,T., Golomb,M. and Riddle,D.L. (1983) RNA polymerase II from wild type and alpha-amanitin-resistant strains of *Caenorhabditis elegans*. *J. Biol. Chem.*, **258**, 12804–12809.
40. Lehrbach,N.J., Castro,C., Murfitt,K.J., Abreu-Goodger,C., Griffin,J.L. and Miska,E.A. (2012) Post-developmental microRNA expression is required for normal physiology, and regulates aging in parallel to insulin/IGF-1 signaling in *C. elegans*. *RNA*, **18**, 2220–2235.
41. Miki,T.S., Richter,H., Rüegger,S. and Großhans,H. (2014) PAXT-1 promotes XRN2 activity by stabilizing it through a conserved domain. *Mol. Cell*, **53**, 351–360.
42. Bosse,G.D., Ruegger,S., Ow,M.C., Vasquez-Rifo,A., Rondeau,E.L., Ambros,V.R., Großhans,H. and Simard,M.J. (2013) The decapping scavenger enzyme DCS-1 controls microRNA levels in *Caenorhabditis elegans*. *Mol. Cell*, **50**, 281–287.
43. Zisoulis,D.G., Kai,Z.S., Chang,R.K. and Pasquinelli,A.E. (2012) Autoregulation of microRNA biogenesis by let-7 and Argonaute. *Nature*, **486**, 541–544.
44. Winter,J. and Diederichs,S. (2011) Argonaute proteins regulate microRNA stability: Increased microRNA abundance by Argonaute proteins is due to microRNA stabilization. *RNA Biol.*, **8**, 1149–1157.
45. Hafner,M., Renwick,N., Brown,M., Mihailovic,A., Holoch,D., Lin,C., Pena,J.T., Nusbaum,J.D., Morozov,P., Ludwig,J. *et al.* (2011) RNA-ligase-dependent biases in miRNA representation in deep-sequenced small RNA cDNA libraries. *RNA*, **17**, 1697–1712.
46. Jorgensen,E.M. and Mango,S.E. (2002) The art and design of genetic screens: *Caenorhabditis elegans*. *Nat. Rev. Genet.*, **3**, 356–369.
47. Kamath,R.S., Martinez-Campos,M., Zipperlen,P., Fraser,A.G. and Ahringer,J. (2001) Effectiveness of specific RNA-mediated interference through ingested double-stranded RNA in *Caenorhabditis elegans*. *Genome Biol.*, **2**, RESEARCH0002.
48. Ding,X.C., Slack,F.J. and Großhans,H. (2008) The let-7 microRNA interfaces extensively with the translation machinery to regulate cell differentiation. *Cell Cycle*, **7**, 3083–3090.
49. Wei,X., Potter,C.J., Luo,L. and Shen,K. (2012) Controlling gene expression with the Q repressible binary expression system in *Caenorhabditis elegans*. *Nat. Methods*, **9**, 391–395.
50. Bacaj,T. and Shaham,S. (2007) Temporal control of cell-specific transgene expression in *Caenorhabditis elegans*. *Genetics*, **176**, 2651–2655.
51. Calixto,A., Ma,C. and Chalfie,M. (2010) Conditional gene expression and RNAi using MEC-8-dependent splicing in *C. elegans*. *Nat Methods*, **7**, 407–411.
52. Gaudet,J. and Mango,S.E. (2002) Regulation of organogenesis by the *Caenorhabditis elegans* FoxA protein PHA-4. *Science*, **295**, 821–825.